

# Ab Initio Treatment of Collective Correlations and the Neutrinoless Double Beta Decay of $^{48}\text{Ca}$

J. M. Yao,<sup>1,\*</sup> B. Bally,<sup>2,†</sup> J. Engel,<sup>2,‡</sup> R. Wirth,<sup>1,§</sup> T. R. Rodríguez,<sup>3,¶</sup> and H. Hergert<sup>1,4,\*\*</sup>

<sup>1</sup>Facility for Rare Isotope Beams, Michigan State University, East Lansing, MI 48824-1321

<sup>2</sup>Department of Physics and Astronomy, University of North Carolina, Chapel Hill, North Carolina 27516-3255, USA

<sup>3</sup>Departamento de Física Teórica y Centro de Investigación Avanzada en Física Fundamental,  
Universidad Autónoma de Madrid, E-28049 Madrid, Spain

<sup>4</sup>Department of Physics & Astronomy, Michigan State University, East Lansing, MI 48824-1321

(Dated: November 13, 2021)

Working with Hamiltonians from chiral effective field theory, we develop a novel framework for arbitrary deformed medium-mass nuclei by combining the in-medium similarity renormalization group with the generator coordinate method, which we use to build collective correlations into reference states that are the basis for subsequent renormalization-group evolution. We use the generator coordinate method a second time to diagonalize the evolved Hamiltonian, and compute the double-beta matrix element that governs the neutrinoless double beta decay of  $^{48}\text{Ca}$  to  $^{48}\text{Ti}$ , which we find to have the value 0.61, smaller than the predictions of most phenomenological methods.

**Introduction.** The discovery that neutrinos oscillate [1–4] and thus have mass has increased the significance of neutrinoless double beta ( $0\nu\beta\beta$ ) decay [5], a hypothetical rare nuclear transition in which a parent nucleus decays into a daughter with two fewer neutrons and two more protons, while emitting two electrons but no (anti)neutrinos. The search for this lepton-number-violating process has become a priority in nuclear and particle physics; its observation would have fundamental implications for the nature of neutrinos, physics beyond the Standard Model, and cosmology.

$0\nu\beta\beta$  decay can be caused by the exchange of heavy particles in theories that violate lepton number, but whatever the cause, a nonzero decay rate implies a contribution from the exchange of a light Majorana neutrino, and we focus on that contribution here. If it is the dominant one the inverse  $0\nu\beta\beta$  half life can be written in the form,

$$[T_{1/2}^{0\nu}]^{-1} = g_A^4 G_{0\nu} \left| \frac{\langle m_{\beta\beta} \rangle}{m_e} \right|^2 |M^{0\nu}|^2 \quad (1)$$

where  $m_e$  is electron mass and  $g_A$  the axial-vector coupling constant. The phase-space factor  $G_{0\nu} \sim 10^{-14}\text{yr}^{-1}$  can be evaluated precisely [6–8]. The effective Majorana neutrino mass  $\langle m_{\beta\beta} \rangle = |\sum_k U_{ek}^2 m_k|$  contains physics beyond the standard model through the masses  $m_k$  and the elements  $U_{ek}$  of the Pontecorvo-Maki-Nakagawa-Sakata (PMNS) matrix that mixes neutrino flavors. Certain combinations of these parameters have been measured, but we still do not know the individual masses  $m_k$  and the combination  $m_{\beta\beta}$ . Equation (1) provides a way to determine  $\langle m_{\beta\beta} \rangle$  from a measured half life (which must be significantly longer than that of any other process ever observed) if the nuclear matrix element (NME)  $M^{0\nu}$  is known. Since the NME cannot be measured, a first-principles calculation is crucial.

Formulating the calculation is straightforward. The NME  $M^{0\nu} = \langle F | O^{0\nu} | I \rangle$ , where  $F$  and  $I$  label the ground states of the final and initial nuclei, involves a transition operator that in

the closure approximation is [9]

$$O^{0\nu} = \frac{4\pi R}{g_A^2} \int d^3r_1 d^3r_2 \int \frac{d^3q}{(2\pi)^3} \frac{e^{i\mathbf{q}\cdot(\mathbf{r}_1-\mathbf{r}_2)}}{q(q+E_d)} \mathcal{J}_\mu^\dagger(\mathbf{r}_1) \mathcal{J}^{\mu\dagger}(\mathbf{r}_2). \quad (2)$$

Here  $R = 1.2A^{1/3}$  is the nuclear radius given by the mass number  $A$ ,  $\mathbf{q}$  is the momentum transfer,  $\mathcal{J}_\mu^\dagger$  is the nuclear current operator, and  $E_d$  is an average excitation energy, to which the matrix element is not sensitive. We neglect short-range effects that are often mocked up by Jastrow functions, the effects of which are small, and also neglect for now very-high energy virtual neutrinos and meson exchanges that induce additional operators in chiral effective field theory [10, 11]. Although it is easy to specify what to calculate, the NMEs predicted by nuclear models differ from one another by factors of up to three, leading to an uncertainty of about an order of magnitude (at least) in the half-life, given a value of  $m_{\beta\beta}$  [12]. It is difficult to reduce this uncertainty because each model has its own phenomenology and uncontrolled approximations. Several groups have therefore begun programs to calculate the NMEs from first principles, taking advantage of a flowering of *ab initio* nuclear-structure theory in the last couple of decades [13–19]. Applying the new *ab initio* methods to  $\beta\beta$  decay, however, poses a major challenge. The nuclei that are used in experiment are generally heavier and more structurally complicated than those examined so far, and the  $0\nu\beta\beta$  NME entails a much more involved calculation than do expectation values of the Hamiltonian or other simple observables. Recently, *ab initio* quantum Monte Carlo methods have been used to calculate NMEs [20], but only in very light nuclei that are not of interest to experimentalists.

Among the *ab initio* methods that can be applied to heavier nuclei, the in-medium similarity renormalization group (IMSRG) [21, 22], seems particularly promising because the time and memory required to complete a calculation depend polynomially on the size of the single-particle basis used, and only indirectly on the nuclear mass. Like the related coupled-cluster approach [17], the method has thus far been applied only to spherical nuclei. Here, we extend the IMSRG to de-

formed nuclei by combining it with the generator coordinate method (GCM) [23, 24], which successfully describes nuclei with complex shapes in nuclear density functional theory [25–27]. We apply the new approach to compute the NME for the  $0\nu\beta\beta$  decay of  $^{48}\text{Ca}$  to the deformed nucleus  $^{48}\text{Ti}$ . Our method is *ab initio* in that it starts from a two-nucleon ( $2N$ ) plus three-nucleon ( $3N$ ) interaction that is derived from chiral effective field theory, with parameters fit in the lightest nuclei, and proceeds through a series of steps that with enough computing power would constitute an exact solution of the resulting Schrödinger equation.  $^{48}\text{Ca}$  makes for a useful first application because it is the lightest candidate nucleus for an experiment, and a program to use it already exists [28].

*Methods.* We employ a Hamiltonian, with the center-of-mass piece subtracted off, that has the form

$$H = \left(1 - \frac{1}{A}\right) \sum_i \frac{p_i^2}{2m} - \sum_{i<j} \frac{\mathbf{p}_i \cdot \mathbf{p}_j}{Am} + \sum_{i<j} V_{ij}^{(2N)} + \sum_{i<j<k} V_{ijk}^{(3N)}. \quad (3)$$

$V^{(2N)}$  is the next-to-next-to-next-to leading order ( $N^3\text{LO}$ ) two-nucleon interaction with initial cutoff  $\Lambda = 500 \text{ MeV}/c$  of Entem and Machleidt [29], evolved to a resolution scale  $\lambda = 1.8 \text{ fm}^{-1}$  or  $\lambda = 2.0 \text{ fm}^{-1}$  by the free-space SRG [30]. The accompanying next-to-next-to-leading order ( $N^2\text{LO}$ )  $3N$  interaction is constructed directly at a chiral cutoff of  $\Lambda = 2.0 \text{ fm}^{-1}$ , to avoid carrying out  $3N$  SRG evolution. It is stipulated that the evolution's effects can be absorbed into the low-energy constants  $c_D$  and  $c_E$ , which are tuned to reproduce the triton binding energy and the charge radius of  $^4\text{He}$  [31, 32]. We will refer to these interactions as  $\text{EM}\lambda/\Lambda$ , e.g.,  $\text{EM}1.8/2.0$ . In working with  $V^{(3N)}$ , we drop beyond-two-body terms after normal-ordering with respect to an  $A = 48$  reference state, in a procedure that defines the normal-ordered two-body (NO2B) approximation. We also drop three-body matrix elements involving states whose single-particle energies  $e_i$  (in units of  $\hbar\omega$ , the harmonic-oscillator spacing for our working basis) sum to  $e_1 + e_2 + e_3 > E_{3\text{max}} = 14$ .

Starting from the Hamiltonian (3), we use the Hartree-Fock-Bogoliubov (HFB) method, with variation after particle-number projection, to find the best quasiparticle vacua that include correlations due to pairing and axial deformation with well-defined parity in both  $^{48}\text{Ca}$  and  $^{48}\text{Ti}$ . Such correlations are hard to generate in the particle-hole-like expansion picture underlying the IMSRG and related methods [22, 33, 34], which is why these states are ideal complementary starting points for the IMSRG evolution of operators (see Refs. [18, 35–38] for other approaches to this issue). Because our matrix-element calculation requires the ground states of both nuclei, we extend ideas from Ref. [39] to correlated states. We employ a mixed (ensemble) reference state defined by a density operator  $\rho = \sum_{\alpha=L,F} c_\alpha |\Phi_\alpha\rangle\langle\Phi_\alpha|$ , where the  $|\Phi_\alpha\rangle$  are the symmetry-restored states with  $J^\pi = 0^+$ , obtained by projecting the lowest-energy quasiparticle vacua in each nucleus onto good angular momentum as well as particle number, and  $c_I + c_F = 1$ . As we show later, we can vary the mixing coefficients  $c_\alpha$  widely without affecting the com-

puted NME. Having fixed our reference ensemble, we normal order the Hamiltonian (3) with respect to it by using the techniques of Refs. [40, 41] and decouple it from all its number-conserving excitations by applying a unitary transformation  $U(s) = e^{\Omega(s)}$ , where  $\Omega(s)$  is an anti-Hermitian many-body operator determined by the flow equation [42]

$$\frac{d\Omega(s)}{ds} = \sum_{n=0}^{\infty} \frac{B_n}{n!} \text{ad}_{\Omega(s)}^k(\eta(s)), \quad (4)$$

and  $s$  is a time-like flow parameter that becomes large during the flow. Here, the  $B_{n=0,1,2,\dots}$  are the Bernoulli numbers,  $\text{ad}_{\Omega}^k(\eta) = [\Omega, \text{ad}_{\Omega}^{k-1}(\eta)]$  with  $\text{ad}_{\Omega}^0(\eta) = \eta$ , and  $\eta(s)$  is the generator of the IMSRG transformation. We use the Brillouin generator [22], which is essentially the gradient of the energy with respect to the parameters that specify the local  $s$ -dependent transformation. Using  $\Omega(s)$ , we can construct any transformed operator  $O(s)$  via

$$O(s) = e^{\Omega(s)} O e^{-\Omega(s)} = \sum_{n=0}^{\infty} \frac{1}{n!} \text{ad}_{\Omega}^k(O), \quad (5)$$

truncating all operators at the NO2B level.

Because our reference ensemble contains projected quasiparticle vacua in both  $^{48}\text{Ca}$  and  $^{48}\text{Ti}$ , neither of those states alone is an eigenvector of the transformed Hamiltonian, but both should be reasonable approximations. (The point of using an ensemble reference is to obtain a single set of operators, rather than a set for each nucleus as in Ref. [43].) Because the IMSRG evolution eliminates components in which just a few particles are excited, we should be able to obtain close-to-exact eigenvectors of the evolved Hamiltonian by admixing states that differ in their *collective* correlations. Thus, we use the evolved Hamiltonian to carry out a second set of projected-HFB calculations, which generate an entire group of number-projected quasiparticle vacua  $|\Phi_{ZN}(\mathbf{Q})\rangle$  with  $\mathbf{Q} = \{q_{2\mu}, \phi_{np}\}$  representing quadrupole moments  $q_{2\mu} = \langle\Phi_{ZN}(\mathbf{Q})|r^2 Y_{2\mu}|\Phi_{ZN}(\mathbf{Q})\rangle$  and an isoscalar (proton-neutron) pairing amplitude  $\phi_{np} = \langle\Phi_{ZN}(\mathbf{Q})|P_0^\dagger|\Phi_{ZN}(\mathbf{Q})\rangle + \langle\Phi_{ZN}(\mathbf{Q})|P_0|\Phi_{ZN}(\mathbf{Q})\rangle$ . Here, we define the isoscalar pairing operator as [44]

$$P_0^\dagger \equiv \frac{1}{\sqrt{2}} \sum_{\ell} \hat{\ell} [a_{\ell}^\dagger a_{\ell}^\dagger]_{000}^{L=0, J=1, T=0}, \quad (6)$$

where  $\hat{\ell} \equiv \sqrt{2\ell+1}$ , and  $L, J, T$  are the coupled orbital angular momentum, total angular momentum, and isospin of the proton-neutron pair (with the zero subscripts representing  $z$  projections). We construct low-lying states by further projecting the number-projected quasiparticle vacua onto states with well defined angular momentum  $J$ ,  $|JMZN(\mathbf{Q}_i)\rangle \equiv P_{M0}^J |\Phi_{ZN}(\mathbf{Q}_i)\rangle$  (there is no need for  $K$ -mixing since axial symmetry is preserved), and superposing the fully projected states via the GCM,

$$|\Psi^{JMZN}\rangle = \sum_{\mathbf{Q}_i} F^{JMZN}(\mathbf{Q}_i) |JMZN(\mathbf{Q}_i)\rangle, \quad (7)$$

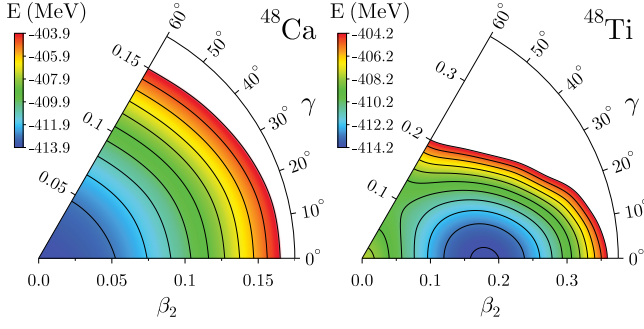


FIG. 1. The particle-number projected potential energy surfaces of  $^{48}\text{Ca}$  and  $^{48}\text{Ti}$  in the deformation  $(\beta_2, \gamma)$  plane for the interaction EM1.8/2.0 with  $e_{\text{max}} = 8$ ,  $\hbar\omega = 16$  MeV (see text). Neighboring contour lines are separated by 1 MeV.

The weights  $F^{JZN}(\mathbf{Q}_i)$  are determined by the variational principle, which leads to the Hill-Wheeler-Griffin equation [24]. To solve this equation, we first diagonalize the norm matrix and construct the orthonormal *natural* basis by removing states with eigenvalues below some cutoff value. Then, we diagonalize the Hamiltonian in the reduced subspace.

We note that because we are always using Hamiltonians in our approach, we do not suffer from spurious divergences and discontinuities that affect GCM applications based on nuclear energy density functionals [45, 46].

**Results and discussion.** Figure 1 displays the potential energy surfaces for  $^{48}\text{Ca}$  and  $^{48}\text{Ti}$  in the plane of deformation parameters  $(\beta_2, \gamma)$  that are produced by the second set of number-projected quasiparticle vacua, before angular-momentum projection. The underlying IMSRG-evolved Hamiltonian comes from the EM1.8/2.0 interaction with  $e_{\text{max}} = 8$  and  $\hbar\omega = 16$  MeV. The quadrupole-deformation parameters are defined as  $\beta_2 \equiv 4\pi/(3AR_0^2)\sqrt{q_{20} + 2q_{22}}$  with  $R_0 = 1.2A^{1/2}$ , where  $A$  is the mass number, and  $\gamma \equiv \arctan \sqrt{2}q_{22}/q_{20}$ . For convenience, we use the bare rather than the evolved quadrupole operators to define  $\beta_2$  and  $\gamma$ ; this has no effect on our computed observables. The figure shows that  $^{48}\text{Ca}$  has a pronounced energy minimum at a spherical shape, and that the energy of  $^{48}\text{Ti}$  has a similarly pronounced minimum at a prolate shape with  $\beta_2 \sim 0.2$  and  $\gamma = 0.0$ . The effect of triaxiality on the low-lying states of both nuclei and on the NME should be negligible.

We compute all quantities with the chiral interactions discussed above, and with a range of values for  $e_{\text{max}}$  and  $\hbar\omega$  (see supplemental material for details.) For the EM1.8/2.0 interaction, which produces satisfactory ground-state and separation energies through mass  $A \sim 80$  [47–49], we obtain extrapolated ground state energies of -418.26 MeV and -422.27 MeV for  $^{48}\text{Ca}$  and  $^{48}\text{Ti}$ , respectively. Our calculation reproduces the ordering for the ground states of the two nuclei, but our  $Q$ -value  $Q_{\beta\beta} = 5.57$  MeV is somewhat larger than the experimental value 4.26 MeV.

Figure 2 shows the low-lying spectrum of  $^{48}\text{Ti}$  for the same interactions. The spectrum is clearly rotational, though

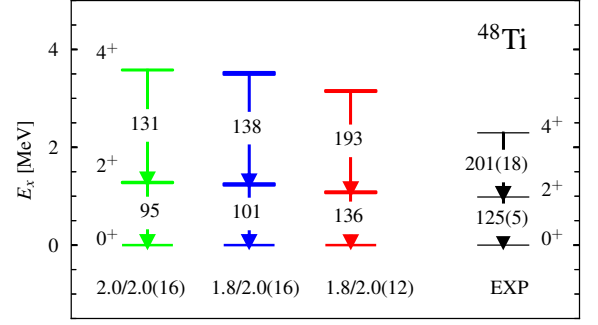


FIG. 2. The low-lying energy spectrum in  $^{48}\text{Ti}$  from the IM-SRG+GCM calculation, with interactions and oscillator frequencies labeled EM $\lambda/\Lambda(\hbar\omega)$ . The rightmost column contains experimental data [50].

slightly stretched. Importantly, we reproduce the collective  $B(E2 : 2_1^+ \rightarrow 0_1^+)$  reasonably well in all cases. The inclusion of non-collective configurations from isoscalar pairing, not shown in the figure, slightly compresses the spectra and changes the  $B(E2 : 2_1^+ \rightarrow 0_1^+)$  by 5-6%, e.g., from 101  $e^2 \text{fm}^4$  to 96  $e^2 \text{fm}^4$  for the EM1.8/2.0 interaction.

The energies of the low-lying states are converged to within a few percent with respect to the basis size (see supplemental material). For example, the excitation energies of the  $2^+$  states in  $^{48}\text{Ti}$  obtained with EM1.8/2.0 or EM2.0/2.0 with  $\hbar\omega = 16$  MeV differ by no more than 3% from  $e_{\text{max}} = 6$  through  $e_{\text{max}} = 10$ . For other observables, the convergence is less obvious. The part of the E2 operator induced by the IMSRG flow alters the  $B(E2)$ 's by less than 10%, suggesting that the matrix elements of this long-range operator are baked into the reference ensemble. We thus do not expect the differences between the E2's in the middle two spectra to be significantly reduced by expanding the number of shells. Surprisingly, even a drastic change of the coefficients ( $c_I, c_F$ ) that specify the contributions of  $^{48}\text{Ca}$  and  $^{48}\text{Ti}$  in the reference ensemble from (0.5, 0.5) to (0.1, 0.9) changes the g.s. energy by a mere 100-200 keV, excited states by 5% or less, and the  $B(E2)$  by only 1%.

TABLE I. The NME  $M^{0\nu}$  for the decay  $^{48}\text{Ca} \rightarrow ^{48}\text{Ti}$  from the IM-SRG+GCM calculation. The results labeled by  $^*/\dagger$  are from non-standard reference ensembles with mixing weights (1/3, 2/3) and (0.1, 0.9), respectively. For other cases the weights are (1/2, 1/2).

Interaction	$\hbar\omega$	NME		
		$e_{\text{max}} = 6$	$e_{\text{max}} = 8$	$e_{\text{max}} = 10$
EM1.8/2.0	12	0.85	0.70	0.64
EM1.8/2.0	16	1.03	0.78	0.66
EM2.0/2.0	16	1.02	0.68	0.75
EM1.8/2.0*	16		0.81	
EM1.8/2.0†	16		0.80	

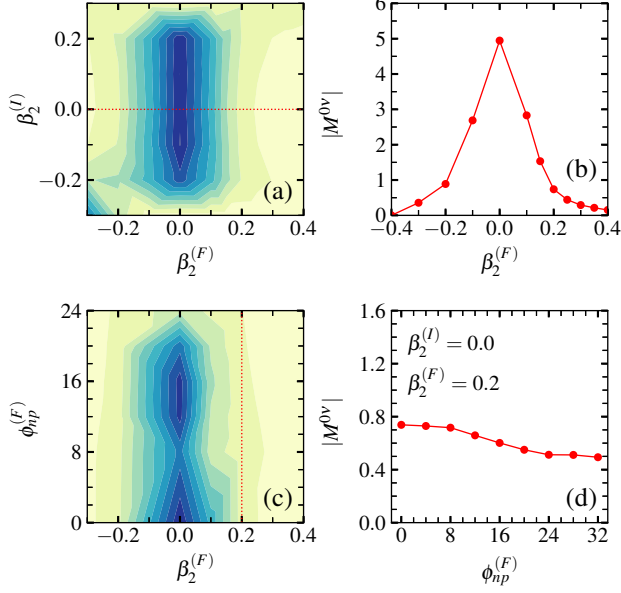


FIG. 3. (a) Contributions to the NME  $|M^{0\nu}|$  in the  $(\beta_2^{(I)}, \beta_2^{(F)})$  plane. Neighboring contour lines here and in (c) are separated by 0.50. (b) The NME  $|M^{0\nu}|$  as a function of the quadrupole deformation parameter  $\beta_2^{(F)}$  in  $^{48}\text{Ti}$ . (c) Contributions to  $|M^{0\nu}|$  in the  $(\beta_2^{(F)}, \phi_{pn}^{(F)})$  plane. (d) The NME  $|M^{0\nu}|$  as a function of the proton-neutron pairing amplitude  $\phi_{pn}^{(F)}$  in  $^{48}\text{Ti}$ .

We turn now to the  $0\nu\beta\beta$  NME, which we compute with the usual parameterizations of the nuclear current operator [51]. Figure 3 displays contributions to the NME from different deformations in the initial and final nuclides. Panel (a) shows that the contribution depends hardly at all on the initial deformation  $\beta_2^{(I)}$ , as long as that quantity is between  $-0.2$  and  $0.2$ . But it depends strongly on the final deformation  $\beta_2^{(F)}$ , as panels (a) and (b) both make clear. Panel (b) shows more explicitly that the contribution to the matrix element changes rapidly with  $\beta_2^{(F)}$ ; the significant average deformation of  $^{48}\text{Ti}$  means that the NME will be suppressed. This result echos the findings of multi-reference EDF calculations [52, 53], which show that the NME is strongly quenched if the initial and final nuclei have different shapes.

Figure 3 (c) and (d) illustrate how the NME is affected by isoscalar pairing, which was shown to have a significant impact in valence-space GCM calculations with empirical interactions [54], [55]. The ground state of  $^{48}\text{Ti}$ , as we have seen, is dominated by configurations with  $\beta_2^{(F)}$  around  $0.2$ , and at that value the isoscalar pairing is significantly smaller than in spherical configurations. The overall effect of isoscalar pairing on the matrix element is thus quite mild, as panel (d) shows. (Isoscalar pairing in  $^{48}\text{Ca}$  is negligible.)

Because the impact of isoscalar pairing is limited and because large-scale GCM calculations with EDFs find cancellations when isovector pairing fluctuations are considered [58], we present results without using the isoscalar-pairing ampli-

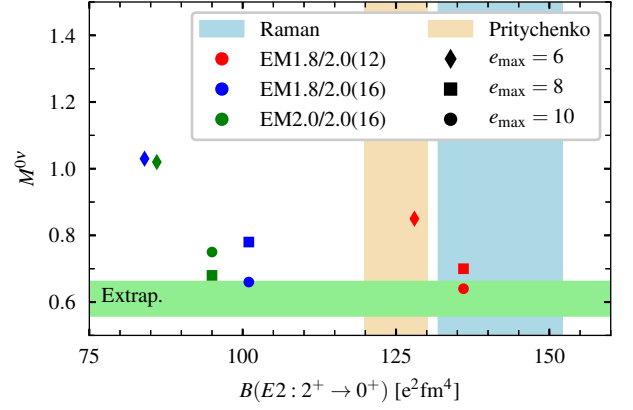


FIG. 4. The NME  $M^{0\nu}$  versus the  $B(E2 : 2_1^+ \rightarrow 0_1^+)$  value in  $^{48}\text{Ti}$  from IMSRG+GCM calculation, with different interactions, oscillator frequencies, and cutoffs. The vertical shaded areas indicate the experimental  $B(E2 : 2_1^+ \rightarrow 0_1^+)$  values for  $^{48}\text{Ti}$  from Refs. [56, 57]. The horizontal area represents the results  $(0.61^{+0.04}_{-0.05})$  of extrapolation.

tude as a generator coordinate for the time being. Table I thus lists the full NMEs from both nuclei with several different interactions. The results in the largest model spaces are relatively close to one another, with NMEs between  $0.64$  and  $0.75$ . All the results are summarized in Fig. 4. There is a noticeable but fairly weak correlation between the NME and the  $B(E2 : 2_1^+ \rightarrow 0_1^+)$  value in  $^{48}\text{Ti}$ , even in the largest model space we consider. To extrapolate to still larger spaces, we perform a Bayesian fit of the parameters in the exponential formula [59]  $M^{0\nu}(e_{\text{Max}}) = M^{0\nu}(\infty) + a \exp(-b \cdot e_{\text{Max}})$ . For the interaction EM1.8/20 with  $\hbar\omega = 16$  MeV, we obtain an extrapolated NME of  $M^{0\nu}(\infty) = 0.57$ , with an extrapolation uncertainty range of  $(+0.08, -0.1)$ ; with  $\hbar\omega = 12$  MeV we get  $0.66$  with a range of  $(+0.03, -0.10)$ . With the constraint that the extrapolated values be the same for both oscillator frequencies, we obtain  $M^{0\nu}(\infty) = 0.61$  with an extrapolation uncertainty range of  $(+0.04, -0.05)$ . All the central values are smaller than the predictions of most phenomenological models. They also carry additional uncertainties, including truncation of the flow equations at the NO2B level, that are hard to quantify at present and will be investigated more closely. We have not included an isoscalar pairing coordinate, which reduces the NME by about 17 % independently of  $e_{\text{max}}$ , for reasons discussed above. The oscillation with  $e_{\text{max}}$  for EM2.0/2.0 prevents a similar analysis there.

Finally, it is worth commenting on the renormalization of the NME. The effect of the IMSRG flow is significant: With the unevolved  $0\nu\beta\beta$  operator, the NME for EM1.8/2.0 at  $\hbar\omega = 16$  MeV and  $e_{\text{max}} = 8$  is  $0.31$  instead of  $0.78$ . A more careful analysis shows that the flow incorporates the effects of pairing in high-energy orbitals, greatly enhancing the  $J = 0$  contribution to the NME. Breaking down the NME by the distance between the decaying nucleons, we confirm that while the largest contribution comes from a peak around  $1$  fm

(cf. [60]), the NME is not purely of short- or long-range character (see supplemental material). Thus, effects from evolving the initial  $0\nu\beta\beta$  operator to the same resolution scale as the interaction will also need to be considered in future fully consistent calculations.

**Conclusions.** In this Letter, we have reported the first *ab-initio* calculation of the spectrum and transition probabilities in a deformed medium-mass nucleus and significant progress in the *ab initio* computation of the nuclear matrix element for the neutrinoless double- $\beta$  decay of  $^{48}\text{Ca}$ . Our primary tool is a novel multireference method for deformed nuclei that combines IMSRG and GCM. With this approach, we reproduce the low-lying (collective) spectrum of  $^{48}\text{Ti}$  satisfactorily. The first  $B(E2)$  value, which is generated by a long-range operator, is approximately right in our calculation, but with a significant dependence on  $\hbar\omega$  that does not decrease as we enlarge the model space to  $e_{\text{max}} = 10$ . In a way this result confirms the ideas behind our method — that truncations keep the IMSRG from capturing collective correlations, which we obtain by embedding them in the reference state instead. Fortunately, although the NME is correlated with the  $B(E2)$  value, the correlation is not strong.

Our best estimate of the NME with EM1.8/2.0 is  $M^{0\nu} = 0.61$ , while with EM2.0/2.0 it would be a few percent larger. These values are smaller than the predictions of most phenomenological approaches [12]. An isoscalar pairing coordinate reduces the NME by about 17 %, but the effect might be smaller when the calculation also builds in isovector pairing fluctuations [58].

To assign an overall error bar, we will go beyond the NO2B level (see [33] for proof-of-principle results), explore more correlation in the GCM, and consistently treat contributions to the  $0\nu\beta\beta$  operator from higher orders in chiral effective field theory, including many-body currents [61, 62]. We must also treat a leading-order contact operator [10] with a coefficient that is currently unknown. We do not expect any of these steps (with the possible exception of introducing the contact operator) to dramatically change the matrix element, however, and we plan to apply our methods to heavier nuclei, such as  $^{76}\text{Ge}$  and  $^{136}\text{Xe}$ .

**Acknowledgments.** We thank A. Belley, G. Hagen, J. D. Holt, J. Menendez, S. Novario, T. Papenbrock, and R. Stroberg for useful discussions and comments. We also thank the Institute for Nuclear Theory at the University of Washington for its hospitality during the completion of this work. This work is supported in part by the U.S. Department of Energy, Office of Science, Office of Nuclear Physics under Award Numbers DE-SC0017887, DE-FG02-97ER41019, and DE-SC0015376 (the DBD Topical Theory Collaboration). T.R.R. is supported in part by the Spanish MICINN under contract PGC2018-094583-B-I00. Computing resources were provided by the Institute for Cyber-Enabled Research at Michigan State University, the Research Computing group at the University of North Carolina at Chapel Hill, and the U.S. National Energy Research Scientific Computing Center (NERSC), a DOE Office of Science User Facility supported

by the Office of Science of the U.S. Department of Energy under Contract No. DE-AC02-05CH11231.

---

\* yaoj@frib.msu.edu  
† bbally@email.unc.edu  
‡ engelj@physics.unc.edu  
§ wirth@frib.msu.edu  
¶ tomas.rodriguez@uam.es  
\*\* hergert@frib.msu.edu

- [1] Y. Fukuda *et al.* (Super-Kamiokande Collaboration), Phys. Rev. Lett. **81**, 1562 (1998).
- [2] Q. R. Ahmad, *et al.* (SNO Collaboration), Phys. Rev. Lett. **87**, 071301 (2001).
- [3] K. Eguchi, *et al.* (KamLAND Collaboration), Phys. Rev. Lett. **90**, 021802 (2003).
- [4] F. P. An *et al.* (Daya Bay Collaboration), Phys. Rev. Lett. **108**, 171803 (2012).
- [5] W. H. Furry, Phys. Rev. **56**, 1184 (1939).
- [6] J. Kotila and F. Iachello, Phys. Rev. C **85**, 034316 (2012).
- [7] S. Stoica and M. Mirea, Phys. Rev. C **88**, 037303 (2013).
- [8] F. Šimkovic, R. Dvornický, D. Štĕfánik, and A. Faessler, Phys. Rev. C **97**, 034315 (2018).
- [9] S. M. Bilenky and S. T. Petcov, Rev. Mod. Phys. **59**, 671 (1987).
- [10] V. Cirigliano, W. Dekens, J. de Vries, M. L. Graesser, E. Mereghetti, S. Pastore, and U. van Kolck, Phys. Rev. Lett. **120**, 202001 (2018).
- [11] V. Cirigliano, W. Dekens, E. Mereghetti, and A. Walker-Loud, Phys. Rev. C **97**, 065501 (2018).
- [12] J. Engel and J. Menéndez, Rep. Prog. Phys. **80**, 046301 (2017).
- [13] P. Navrátil, S. Quaglioni, I. Stetcu, and B. R. Barrett, Journal of Physics G: Nuclear and Particle Physics **36**, 083101 (2009).
- [14] D. Lee, Prog. Part. Nucl. Phys. **63**, 117 (2009).
- [15] B. R. Barrett, P. Navrátil, and J. P. Vary, Prog. Part. Nucl. Phys. **69**, 131 (2013).
- [16] V. Somà, C. Barbieri, and T. Duguet, Phys. Rev. C **89**, 024323 (2014).
- [17] G. Hagen, T. Papenbrock, M. Hjorth-Jensen, and D. J. Dean, Rep. Prog. Phys. **77**, 096302 (2014).
- [18] K. D. Launey, T. Dytrych, and J. P. Draayer, Prog. Part. Nucl. Phys. **89**, 101 (2016).
- [19] S. Shen, H. Liang, W. H. Long, J. Meng, and P. Ring, arXiv:1904.04977 [nucl-th] (2019).
- [20] S. Pastore, J. Carlson, V. Cirigliano, W. Dekens, E. Mereghetti, and R. B. Wiringa, Phys. Rev. C **97**, 014606 (2018).
- [21] H. Hergert, S. K. Bogner, T. D. Morris, A. Schwenk, and K. Tsukiyama, *Memorial Volume in Honor of Gerald E. Brown*, Physics Reports **621**, 165 (2016).
- [22] H. Hergert, Physica Scripta **92**, 023002 (2016).
- [23] J. J. Griffin and J. A. Wheeler, Phys. Rev. **108**, 311 (1957).
- [24] P. Ring and P. Schuck, *The nuclear many-body problem* (Springer-Verlag, New York, 1980).
- [25] M. Bender and P.-H. Heenen, Phys. Rev. C **78**, 024309 (2008).
- [26] J. M. Yao, J. Meng, P. Ring, and D. Vretenar, Phys. Rev. C **81**, 044311 (2010).
- [27] T. R. Rodríguez and J. L. Egido, Phys. Rev. C **81**, 064323 (2010).
- [28] T. Iida *et al.*, Journal of Physics: Conference Series **718**, 062026 (2016).
- [29] D. R. Entem and R. Machleidt, Phys. Rev. C **68**, 041001 (2003).

- [30] S. Bogner, R. Furnstahl, and A. Schwenk, *Prog. Part. Nucl. Phys.* **65**, 94 (2010).
- [31] K. Hebeler, S. K. Bogner, R. J. Furnstahl, A. Nogga, and A. Schwenk, *Phys. Rev. C* **83**, 031301 (2011).
- [32] A. Nogga, S. K. Bogner, and A. Schwenk, *Phys. Rev. C* **70**, 061002 (2004).
- [33] H. Hergert, J. M. Yao, T. D. Morris, N. M. Parzuchowski, S. K. Bogner, and J. Engel, *Journal of Physics: Conference Series* **1041**, 012007 (2018).
- [34] N. M. Parzuchowski, S. R. Stroberg, P. Navrátil, H. Hergert, and S. K. Bogner, *Phys. Rev. C* **96**, 034324 (2017).
- [35] A. E. McCoy, M. A. Caprio, and T. Dytrych, *Ann. Acad. Rom. Sci. Ser. Chem. Phys. Sci.* **3**, 17 (2018), arXiv:1802.01771 [nucl-th].
- [36] T. Dytrych, K. D. Launey, J. P. Draayer, D. Rowe, J. Wood, G. Rosensteel, C. Bahri, D. Langr, and R. B. Baker, (2018), arXiv:1810.05757 [nucl-th].
- [37] T. Duguet, *J. Phys. G* **42**, 025107 (2015).
- [38] T. Duguet and A. Signoracci, *J. Phys. G* **44**, 015103 (2017).
- [39] S. R. Stroberg, A. Calci, H. Hergert, J. D. Holt, S. K. Bogner, R. Roth, and A. Schwenk, *Phys. Rev. Lett.* **118**, 032502 (2017).
- [40] W. Kutzelnigg and D. Mukherjee, *J. Chem. Phys.* **107**, 432 (1997).
- [41] D. Mukherjee, *Chem. Phys. Lett.* **274**, 561 (1997).
- [42] T. D. Morris, N. M. Parzuchowski, and S. K. Bogner, *Phys. Rev. C* **92**, 034331 (2015).
- [43] J. M. Yao, J. Engel, L. J. Wang, C. F. Jiao, and H. Hergert, *Phys. Rev. C* **98**, 054311 (2018).
- [44] N. Hinohara and J. Engel, *Phys. Rev. C* **90**, 031301 (2014).
- [45] M. Bender, T. Duguet, and D. Lacroix, *Phys. Rev. C* **79**, 044319 (2009).
- [46] T. Duguet, M. Bender, K. Bennaceur, D. Lacroix, and T. Lesinski, *Phys. Rev. C* **79**, 044320 (2009).
- [47] J. Simonis, S. R. Stroberg, K. Hebeler, J. D. Holt, and A. Schwenk, *Phys. Rev. C* **96**, 014303 (2017).
- [48] J. D. Holt, S. R. Stroberg, A. Schwenk, and J. Simonis, (2019), arXiv:1905.10475 [nucl-th].
- [49] G. Hagen, G. R. Jansen, and T. Papenbrock, *Phys. Rev. Lett.* **117**, 172501 (2016).
- [50] National Nuclear Data Center, “NuDat 2 Database,” <https://www.nndc.bnl.gov/nudat2>.
- [51] F. Šimkovic, A. Faessler, V. Rodin, P. Vogel, and J. Engel, *Phys. Rev. C* **77**, 045503 (2008).
- [52] T. R. Rodríguez and G. Martínez-Pinedo, *Phys. Rev. Lett.* **105**, 252503 (2010).
- [53] J. M. Yao, L. S. Song, K. Hagino, P. Ring, and J. Meng, *Phys. Rev. C* **91**, 024316 (2015).
- [54] J. Menéndez, N. Hinohara, J. Engel, G. Martínez-Pinedo, and T. R. Rodríguez, *Phys. Rev. C* **93**, 014305 (2016).
- [55] C. F. Jiao, J. Engel, and J. D. Holt, *Phys. Rev. C* **96**, 054310 (2017).
- [56] S. Raman, C. W. Nestor, and P. Tikkanen, *At.Data Nucl.Data Tables* **78**, 1 (2001).
- [57] B. Pritychenko, M. Birch, B. Singh, and M. Horoi, *At.Data Nucl.Data Tables* **107**, 1 (2016).
- [58] N. L. Vaquero, T. R. Rodríguez, and J. L. Egido, *Phys. Rev. Lett.* **111**, 142501 (2013).
- [59] R. A. Basili, J. M. Yao, J. Engel, H. Hergert, M. Lockner, P. Maris, and J. P. Vary, in preparation (2019).
- [60] J. Menéndez, A. Poves, E. Caurier, and F. Nowacki, *Nuclear Physics A* **818**, 139 (2009).
- [61] L.-J. Wang, J. Engel, and J. M. Yao, *Phys. Rev. C* **98**, 031301 (2018).
- [62] P. Gysbers, G. Hagen, J. D. Holt, G. R. Jansen, T. D. Morris, P. Navrátil, T. Papenbrock, S. Quaglioni, A. Schwenk, S. R. Stroberg, and K. A. Wendt, *Nature Physics* **15**, 428 (2019).

## SUPPLEMENTAL MATERIALS

Structure of  $^{48}\text{Ti}$ 

Table II lists the detailed information on the low-lying states of  $^{48}\text{Ti}$  from IMSRG+GCM calculations by mixing axially deformed configurations. One can see that the low-energy spectra (except for the ground-state energies) and E2 transition strengths are converged rather well at  $e_{\text{max}} = 10$ .

Figure 5 shows the energy surfaces of  $^{48}\text{Ca}$  and  $^{48}\text{Ti}$  in the  $(\beta_2, \phi_{np})$  plane from the calculation using the EM1.8/2.0 interaction. It is seen clearly that the energy minimum is located at  $\beta_2 = 0.0$  and  $\beta_2 = 0.2$  for  $^{48}\text{Ca}$  and  $^{48}\text{Ti}$ , respectively. Besides, the energy surface is rather soft along the neutron-proton isoscalar pairing amplitude  $\phi_{np}$  in both nuclei around the energy minimum. Therefore, the wave functions of their ground states, which are relevant for the NME of the  $0\nu\beta\beta$ , are mainly concentrated along the valley, as illustrated in Fig. 6. We note that the inclusion of  $\phi_{np}$  degree-of-freedom only changes slightly the energies of low-lying states. For  $^{48}\text{Ca}$ , the ground-state energy is changed from -413.86 MeV to -413.87 MeV by the EM1.8/2.0 interaction with  $e_{\text{max}} = 8$  and  $\hbar\omega = 16$  MeV. For  $^{48}\text{Ti}$ , it is changed from -418.22 MeV to -418.23 MeV. This effect decreases the excitation energy of  $2^+$  state from 1.24 MeV to 1.17 MeV, closer to the data. Figure 7 shows the convergence behavior of the ground-state energies as a function of the  $e_{\text{max}}$ . The results are extrapolated with the exponential formula  $E(e_{\text{max}}) = E(\infty) + a \exp(-b \cdot e_{\text{max}})$ . We find  $E(\infty) = -418.26$  MeV for  $^{48}\text{Ca}$  and -422.27 MeV for  $^{48}\text{Ti}$ .

TABLE II. The structural properties of  $^{48}\text{Ti}$  from the IMSRG+GCM calculation with the chiral interactions, in comparison with available data. All energies are in units of MeV and  $B(E2)$  in  $e^2 \text{fm}^4$ . The results with  $*/\dagger$  are from the calculations starting from the ensemble reference state with mixing weight (1/3, 2/3)/(0.1, 0.9). For other cases, (1/2, 1/2) is used.

EM $\lambda/\Lambda(e_{\text{max}}/\hbar\omega)$	$E(0_1^+)$	$E_x(2_1^+)$	$E_x(4_1^+)$	$B(E2 : 2_1^+ \rightarrow 0_1^+)$
EM1.8/2.0(6/16)	-401.97	1.25	3.35	84
EM1.8/2.0(8/16)	-418.22	1.24	3.57	101
EM1.8/2.0(10/16)	-421.48	1.24	3.48	101
EM1.8/2.0(8/16)*	-417.96	1.30	3.62	99
EM1.8/2.0(8/16) $\dagger$	-418.32	1.32	3.71	100
EM1.8/2.0(6/12)	-387.68	1.03	2.90	128
EM1.8/2.0(8/12)	-409.65	1.06	3.10	136
EM1.8/2.0(10/12)	-416.95	1.08	3.14	137
EM2.0/2.0(6/16)	-361.59	1.32	3.48	86
EM2.0/2.0(8/16)	-387.18	1.33	3.63	95
EM2.0/2.0(10/16)	-395.34	1.28	3.58	95
Exp.	-418.70	0.98	2.30	144 [56] 125 [57]

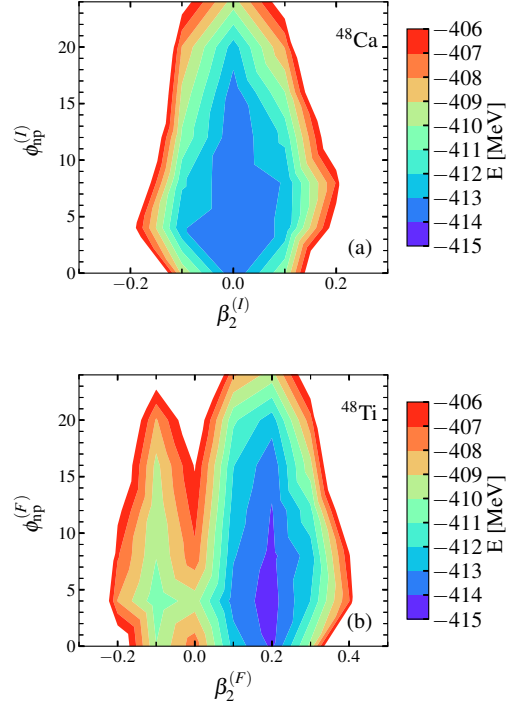


FIG. 5. The particle-number projected potential energy surfaces of  $^{48}\text{Ca}$  and  $^{48}\text{Ti}$  in the  $(\beta_2, \phi_{np})$  plane at  $e_{\text{max}} = 8$ ,  $\hbar\omega = 16$  MeV. The two neighbouring contour lines are separated by 1.0 MeV.

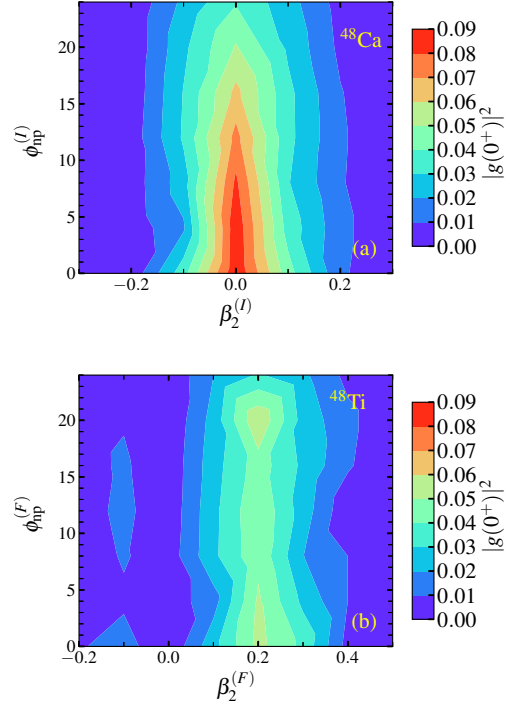


FIG. 6. The collective wave functions of the ground state for  $^{48}\text{Ca}$  and  $^{48}\text{Ti}$  in the  $(\beta_2, \phi_{np})$  plane at  $e_{\text{max}} = 8$ ,  $\hbar\omega = 16$  MeV. The two neighbouring contour lines are separated by 0.01.

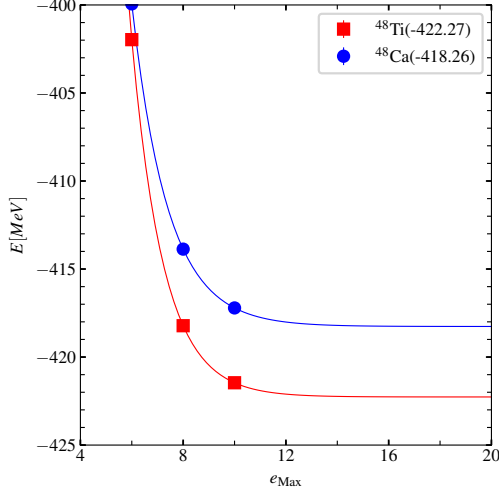


FIG. 7. The ground-state energy from the IMSRG+GCM calculation with the EM1.8/2.0 interaction with oscillator frequency  $\hbar\omega = 16$  MeV as a function of  $e_{\max}$ .

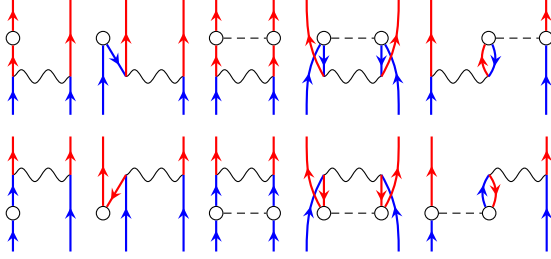


FIG. 8. Antisymmetrized Goldstone diagrams of the leading-order correction  $[\Omega, O^{0\nu}]$  from the IMSRG evolution to the  $0\nu\beta\beta$  decay operator. Hollow dots mark insertions of one- or two-body parts of  $\Omega$ , wavy lines correspond to  $O^{0\nu}$ . The diagrams in the bottom row have to be subtracted. Diagrams containing two-body cumulants cancel and have been omitted. Formulas can be found in Ref. [43].

### IMSRG-Evolved Neutrinoless Double Beta Decay Operator

In the IMSRG flow, the evolved  $0\nu\beta\beta$  decay operator is calculated with the BCH formula,

$$O^{0\nu}(s) = O^{0\nu} + [\Omega(s), O^{0\nu}] + \frac{1}{2}[\Omega(s), [\Omega(s), O^{0\nu}]] + \dots \quad (8)$$

The leading-order correction  $[\Omega(s), O^{0\nu}]$  is illustrated schematically with Goldstone diagrams in Fig. 8. The correction from this term to the operator goes to all the terms in the BCH formula. We find that the contribution from the one-body part (first two columns in Fig. 8) of  $\Omega(s)$  to the commutator  $[\Omega(s), O^{0\nu}]$  is negligible. The contribution of the diagrams in the third and fourth columns enhances the two-body matrix elements, while that of the last column quenches the matrix elements.

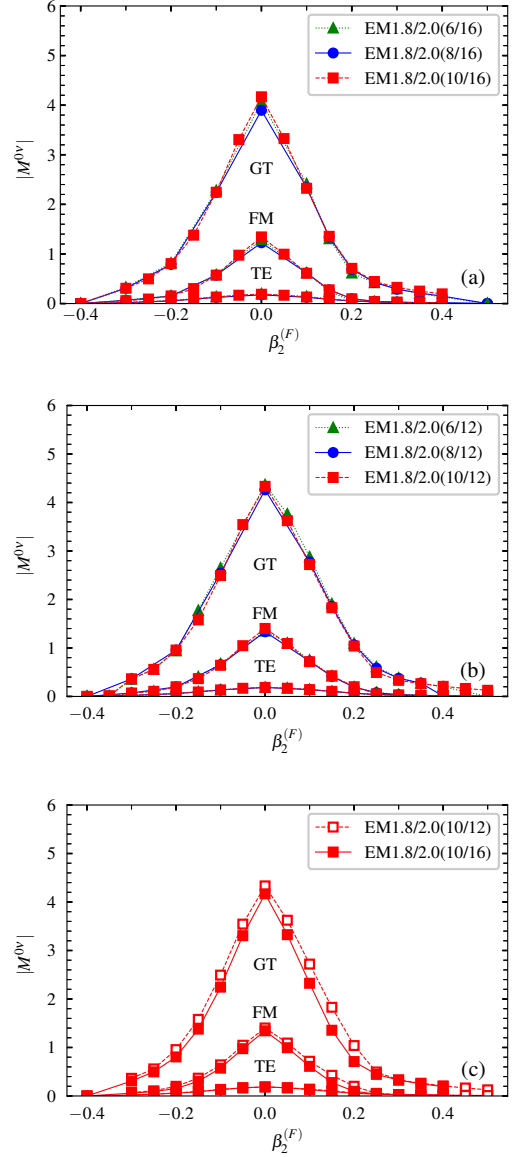


FIG. 9. (a) The normalized NME  $M^{0\nu}$  from the spherical state of  $^{48}\text{Ca}$  to different axially deformed state of  $^{48}\text{Ti}$  from the IMSRG+GCM calculation using EM1.8/2.0( $e_{\max}/16$ ) with  $e_{\max} = 6, 8$ , and  $10$ , respectively; (b) Same as (a) but by the EM1.8/2.0( $e_{\max}/12$ ); (c) Comparison of the results by EM1.8/2.0(10/12) and EM1.8/2.0(10/16).

### Configuration-Dependence of the Nuclear Matrix Element

Figure 9 displays that the NME is very sensitive to the quadrupole deformation of  $^{48}\text{Ti}$ , but not much to the  $e_{\max}$  for a given deformed state with the same  $\beta_2^{(F)}$  value. Moreover, one can see that the NME by  $\hbar\omega = 12$  MeV is systematically larger than that by  $\hbar\omega = 16$  MeV. However, as we find, the  $E2$  transition strengths by the former is also systematically larger than the later. Because of negative correlation between the NME and  $E2$  transition strength, these two interactions pre-

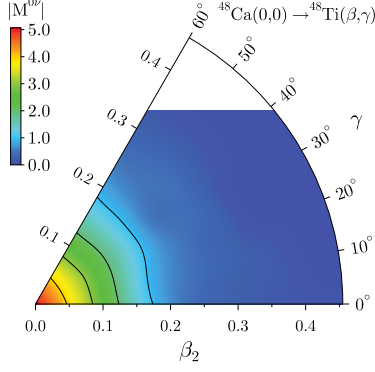


FIG. 10. The configuration-dependence of the NME in the  $(\beta_2, \gamma)$  plane by the EM1.8/2.0(8/16) calculation.

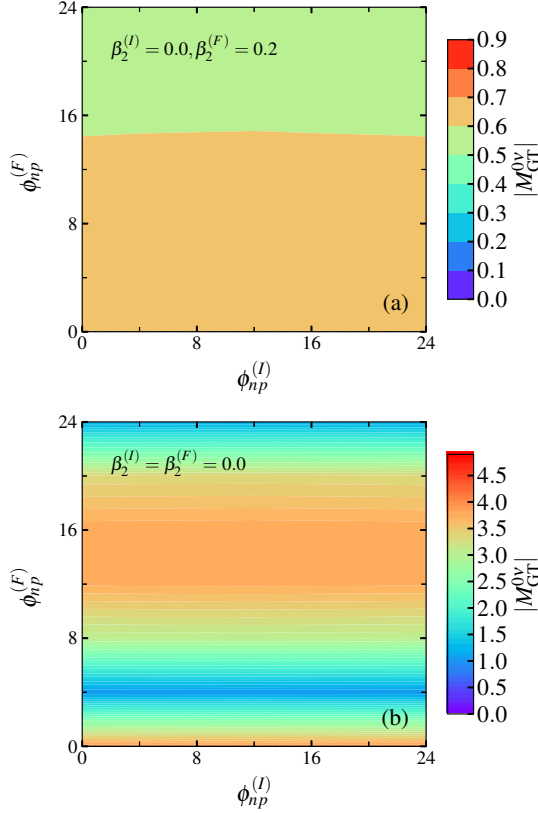


FIG. 11. The configuration-dependence of the NME in the  $(\phi_{np}^{(I)}, \phi_{np}^{(F)})$  plane at  $e_{\max} = 8$ ,  $\hbar\omega = 16$  MeV.

dicts a similar value for the NME in the final IMSRG+GCM calculation.

Figure 10 shows that the NME is insensitive to the triaxial  $\gamma$  deformation of  $^{48}\text{Ti}$ . The inclusion of triaxiality in the GCM calculation is thus expected to be negligible. Figure 11 displays the sensitivity of the NME to the neutron-proton isoscalar pairing amplitude  $\phi_{np}$  in both initial and final nuclei for a given quadrupole deformation parameter. It is seen that the NME is almost independent of  $\phi_{np}^{(I)}$  in  $^{48}\text{Ca}$ , but may vary rapidly with  $\phi_{np}^{(F)}$  in  $^{48}\text{Ti}$ , depending on the  $\beta_2^{(F)}$ .

Table III lists the NME from the IMSRG+GCM calculation with neutron-proton isoscalar pairing fluctuation with  $e_{\max} = 6$  and 8. Compared with the value from the same calculation but without the isoscalar pairing fluctuation, this value is smaller by about 17% in both cases.

### Distance- and Angular-Momentum Dependence of the NME

We can analyze the NME further by breaking it down into contributions from different distances between the decaying nucleons and partial waves. For the former, we introduce the distribution  $C^{0v}(r_{12})$ , defined by

$$M^{0v} = \int_0^\infty dr_{12} C^{0v}(r_{12}), \quad (9)$$

with  $r_{12} = |\mathbf{r}_1 - \mathbf{r}_2|$  the relative distance between the two neutrons that are transformed into protons.

Figure 12 shows distributions of the NME corresponding to the transition from spherical  $^{48}\text{Ca}$  to  $^{48}\text{Ti}$  with different quadrupole deformation and isoscalar pairing amplitude. One can see that the quadrupole correlation quenches the NME in both the long-ranged and short-ranged region. In contrast, the isoscalar pairing quenches the NME mainly in the short-ranged region. The distributions with deformed final states are qualitatively similar to those obtained in phenomenological shell-model calculation of Ref. [60], featuring the appearance of a robust node at  $r_{12} \approx 2.0$  fm.

We decompose the  $C^{0v}(r_{12})$  further into different  $J$  components

$$C^{0v}(r_{12}) = \sum_{\substack{p \leq p' \\ n \leq n'}} \sum_J C_{pp'nn'}^J(r_{12}), \quad (10)$$

where

$$C_{pp'nn'}^J(r_{12}) = \frac{(2J+1)}{\sqrt{(1+\delta_{pp'})(1+\delta_{nn'})}} \times \langle (pp')J | \bar{O}^{0v}(r_{12}) | (nn')J \rangle \rho_{pp'nn'}^J, \quad (11)$$

with  $\langle (pp')J | \bar{O}^{0v}(r_{12}) | (nn')J \rangle$  being the normalized IMSRG evolved two-body transition matrix element in harmonic-

TABLE III. The nuclear matrix element  $M^{0v}$  for the  $0\nu\beta\beta$   $^{48}\text{Ca} \rightarrow ^{48}\text{Ti}$  from the IMSRG+GCM calculation without (w/o) and with (w/) the neutron-proton isoscalar pairing fluctuation using the EM1.8/2.0 interaction and  $\hbar\omega = 16$  MeV. The quenching factor  $q$  is defined as the ratio of the difference in the NMEs to that without  $np$  isoscalar pairing.

$e_{\max}$	$M^{0v}(w/o)$	$M^{0v}(w/)$	$q$
6	1.03	0.86	16.5%
8	0.78	0.65	16.7%

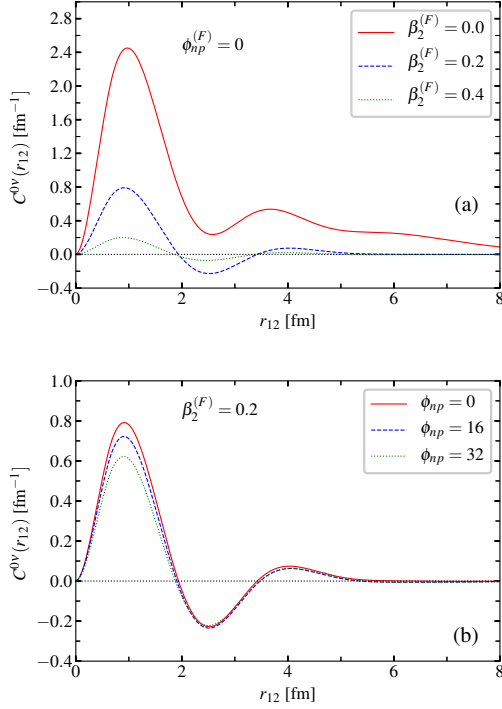


FIG. 12. The distribution of  $C^{0\nu}(r_{12})$  as a function of the relative coordinate  $r_{12}$  corresponding to the transition from spherical  $^{48}\text{Ca}$  to different configuration of  $^{48}\text{Ti}$  by EM1.8/2.0(8/16) distinguished with different values of quadrupole deformation parameter  $\beta_2$  and neutron-proton isoscalar pairing amplitude  $\phi_{np}$ .

oscillator basis and the two-body transition density

$$\rho_{pp'nn'}^J = -\frac{1}{\sqrt{2J+1}} \langle \Psi(^{48}\text{Ti}) | [a_p^\dagger a_{p'}^\dagger]^J [\tilde{a}_n \tilde{a}_{n'}]^J | \Psi(^{48}\text{Ca}) \rangle. \quad (12)$$

Figure 13 displays the  $r$ -dependence of the  $C_{pp'nn'}^J(r_{12})$  from the first six largest two-body transition densities. It is seen that the cancellation between  $J = 0$  and  $J = 2$  components is the main mechanism responsible for the node around  $r_{12} = 2.0$  fm, before and after which point the contribution to the total NME is opposite. It is the large negative contribution from the  $J = 2$  components arising from the strong quadrupole collectivity in  $^{48}\text{Ti}$  quenches the NME strongly.

#### Extrapolation to Infinite Model Space

To get a reliable estimate of the NME extrapolated to infinite model space and its error in the presence of uncertainty in the calculation results, we perform Bayesian inference on the parameters of the exponential formula  $M^{0\nu}(e_{\text{Max}}) = M^{0\nu}(\infty) + a \exp(-b \cdot e_{\text{Max}})$ . The results are displayed in Figure 14. We use normal priors for the extrapolated value ( $\mu = 0.5$ ,  $\sigma = 1$ ) and for the value at  $e_{\text{max}} = 6$ , where the expectation value is set to the central value of the calculation result and we set  $\sigma = 0.2$  to allow for some variation in the extrapolating curve.

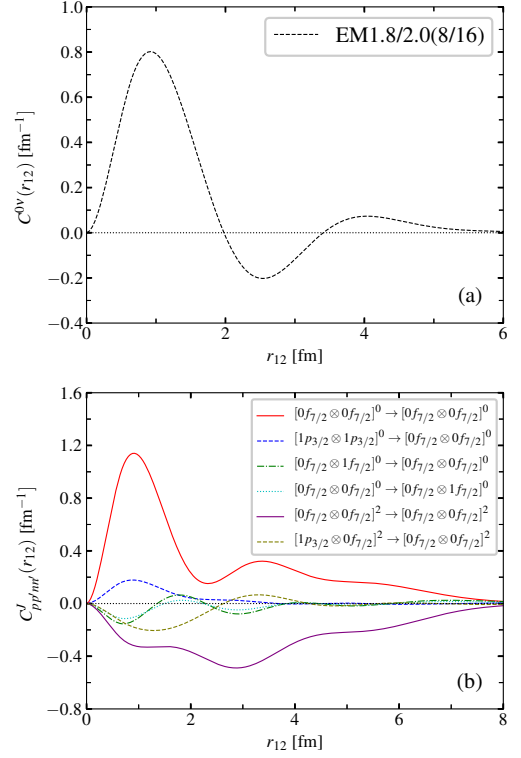


FIG. 13. (a) The distribution of  $C^{0\nu}(r_{12})$  as a function of the relative coordinate  $r_{12}$  from the IMSRG+GCM calculation by EM1.8/2.0(8/16). (b) The contribution from the first six largest two-body transition densities.

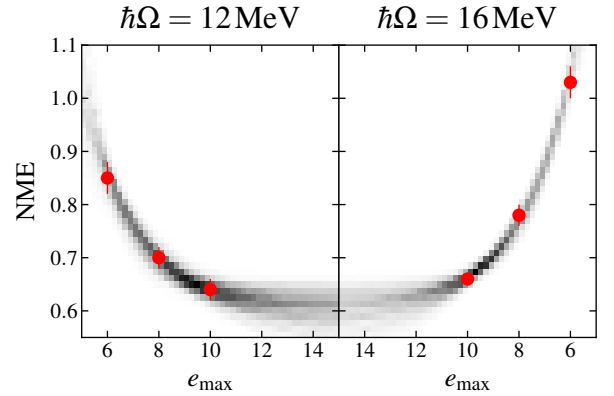


FIG. 14. The NME  $M^{0\nu}$  from the IMSRG+GCM calculation with the EM1.8/2.0 interaction with oscillator frequencies  $\hbar\omega = 12$  MeV and  $\hbar\omega = 16$  MeV as a function of  $e_{\text{max}}$ . The histogram in the background shows the density of 500 realizations of the extrapolating curve drawn from its posterior distribution. Both curves are constrained to yield the same extrapolated value.

The prior for the decay constant is a truncated normal distribution ( $\mu = 0.5$ ,  $\sigma = 2$ ) with the probability density for values less than zero removed in order to get a decaying exponential. We assume Gaussian uncertainties on the resulting values of the NME.

First, we perform inference separately on the  $e_{\max}$  sequences for both oscillator frequencies. The uncertainty on the value of the NME at finite  $e_{\max}$  allows for two solutions, one with a large decay constant and an extrapolated value in the region of 0.6, and one with a small decay constant and very low extrapolated value. This leads to a posterior distribution of the extrapolated value with a very long tail ranging into negative NME values. However, the bulk of the probability is concentrated in a rather small interval. For these reasons, we

use the mode of the posterior as a point estimate and the 68 % highest posterior density credible interval to define its uncertainty. For  $\hbar\omega = 16$  MeV, we get an extrapolated value of 0.57 with an extrapolation uncertainty range of (+0.08, -0.1), the result for  $\hbar\omega = 12$  MeV is 0.66 with extrapolation uncertainty range (+0.03, -0.1). To improve upon this and to get rid of the long tails in the posterior distribution, we also perform a combined fit where the extrapolated value is constrained to be the same for both oscillator frequencies while the other parameters are independent. The inference on the combined data set yields a much more narrow distribution of the extrapolated value and reduces the probability of the slowly decaying solutions. The extrapolated value in this case is 0.61 with an extrapolation uncertainty range (+0.04, -0.05).